Hydrogen-vacancy interaction in tungsten

1991 J. Phys.: Condens. Matter 3 9871

(http://iopscience.iop.org/0953-8984/3/49/004)

J. Phys.: Condens. Matter 3 (1991) 9871–9886. Printed in the UK

Hydrogen–vacancy interaction in tungsten

J R Fransens, M S Abd El Keriem† and F Pleiter

Laboratorium voor Algemene Natuurkunde, Materials Science Centre, University of Groningen, The Netherlands

Received 23 July 1991

Abstract. Hydrogen–vacancy interaction in tungsten was investigated by means of the perturbed angular correlation technique, using the isotope ^{111}In as a probe. Hydrogen trapping at an ^{111}In–vacancy cluster manifests itself as a change of the local electric field gradient, which gives rise to an observable shift of the quadrupole frequency. The measurements show that a vacancy in tungsten can trap one or two hydrogen atoms at room temperature. The detrapping energies of the first and second hydrogen atom are 1.55(2) and 1.38(2) eV, respectively, while the detrapping energy of the next hydrogen atom is less than 1.1 eV. Substitutional ^{111}In atoms do not trap hydrogen at room temperature. At least two more hydrogen decorated defects were observed. Although their structures are not quite clear, they probably form from larger vacancy clusters and may contain a large amount of hydrogen. The dissociation energy of these bubble-like defects is 1.30(2) eV.

1. Introduction

Hydrogen and hydrogen–defect interactions in metals have many technological implications. They have, therefore, been the subject of numerous experimental as well as theoretical studies. Some points of interest in these investigations were the strength of the hydrogen–vacancy binding, the lattice location of hydrogen, and the number of hydrogen atoms that can be accommodated by a single vacancy.

The effective-medium theory has proven to be extremely useful to calculate positions of hydrogen isotopes at lattice defects and the corresponding binding energies. This theory has recently been applied to the case of hydrogen–vacancy binding in a number of transition metals (Nordlander *et al* 1986, 1989). The results obtained for the BCC metals Fe, Nb, Mo and W are collected in table 1.

Hydrogen decoration of monovacancies in molybdenum has been studied experimentally by using the positron lifetime technique (Hansen *et al* 1985, Linderoth *et al* 1987). After the samples had been electrolytically doped with hydrogen, a decrease of the longer lifetime from 180 to 165 ps was observed. It was concluded that either the vacancies had trapped two hydrogen atoms, or that the hydrogen occupancy varied from zero to four. In our opinion, the results of the positron lifetime measurements merely allow us to conclude that vacancies in molybdenum may trap up to several hydrogen atoms. The change in positron lifetime during a thermal annealing sequence was also used to monitor the dissociation of hydrogen–vacancy complexes, yielding a

† On leave from Ain Shams University, Cairo, Egypt.

0953-8984/91/499871+16$03.50

detrapping energy of $E_d = 1.75(5)$ eV. Assuming a value of 0.35 eV for the migration energy, a binding energy $E_b = 1.4(1)$ eV was derived. A comparison of doped and undoped samples, both annealed at 600 K, gave indications that hydrogen-occupied vacancies act as nucleation centres for further vacancy trapping. Comparing measured and calculated positron lifetimes, it was concluded that each cluster may contain 10–30 vacancies.

The binding energy of deuterium at vacancies in molybdenum was derived from deuterium depth profiles measured after subsequent annealing treatments (Myers and Besenbacher 1986). The data had to be fitted with as many as 19 coupled differential equations in order to account for the different deuterium–trap combinations. The analysis yielded a value of 1.03 eV for the binding energy of a deuterium atom at a vacancy, and a value of 0.80 eV for the binding energy at a deuterium-decorated vacancy.

A theoretical investigation of the binding of hydrogen at octahedral and tetrahedral positions in V, Cr, Fe, Nb and Ta showed that the tetrahedral lattice position is slightly favoured, except in the case of Fe (Puska and Nieminen 1984). These calculations allowed for lattice relaxation.

Experimental information about lattice location has been obtained from channelling experiments. In Fe, deuterium is displaced by 0.4 Å from the octahedral site towards a regular lattice site, and in V by 0.4 Å from the octahedral towards the tetrahedral site (Besenbacher *et al* 1985). Deuterium implanted at 87 K in Cr, Mo and W is located within 0.3 Å from the tetrahedral site (Picraux and Vook 1974, Picraux 1976). Upon annealing, however, deuterium in Cr and Mo moves to a position near the octahedral site, the displacement being 0.4 Å towards the vacancy in the case of Cr and 0.2 Å towards the tetrahedral site in the case of Mo. In more recent channelling measurements on V, Cr, Fe, Nb, Mo, Ta and W it was found that deuterium is displaced by about 0.2 Å from the tetrahedral towards the octahedral site in all cases (Ligeon *et al* 1986). The discrepancy between these results can be reconciled if one assumes that in some cases the lattice position was determined by the presence of vacancies and in others it was not.

From this overview the following points become clear.

(i) Hydrogen in BCC metals traps at vacancies.

(ii) A single vacancy may trap up to several hydrogen atoms. However, there is no precise experimental information available about the number of trapped hydrogen atoms.

(iii) The lattice position of hydrogen trapped at a vacancy seems to vary from element to element.

In this article we report on an experiment in which we applied the perturbed angular correlation technique to monitor the number of hydrogen atoms trapped at a vacancy in tungsten. Several problems that hamper the interpretation of the experiments mentioned previously could be circumvented in our approach. As will be shown, we are able to set up a unique and reproducible trap, whereas in channelling experiments the exact nature of the trap is unknown. We can determine the implanted hydrogen dose very accurately by injecting hydrogen atoms with the aid of a low-energy ion gun, contrary to the case when samples are electrochemically loaded. By this procedure we do not introduce new damage into the crystal. Finally, the perturbed angular correlation technique is very sensitive to the number of trapped hydrogen atoms, contrary to all methods mentioned previously. Some preliminary

results of this work have been published before (Post and Pleiter 1987, Fransens *et al* 1988).

2. Trapping of mobile atoms at unsaturable traps

In this section we will briefly discuss the trapping of implanted gas atoms at non-saturable traps. To simplify the picture, we will make a few assumptions which, however, are not necessarily valid in all cases. A more thorough discussion of the trapping theory can be found in the literature (Van Gorkum and Kornelsen 1979, Van Veen and Caspers 1980).

The number of particle–trap encounters during a time interval $\mathrm{d}t$, within a layer with an area $\mathrm{d}S$ and a thickness $\mathrm{d}x$, is equal to the product of (i) the average number of jumps performed by the mobile particle, (ii) the number of mobile particles in the layer and (iii) the relative number of traps:

$$\nu \,\mathrm{d}t\, c(x)\, \mathrm{d}S\, \mathrm{d}x\, zn(x)/N_0 \tag{1}$$

where ν is the jump frequency, $c(x)$ is the steady-state concentration of mobile particles, $n(x)$ is the trap concentration, and N_0 is the atomic density. The factor z in equation (1) is related to the effective trapping radius for the trapping process. The number of impinging particles is

$$J\mathrm{d}S\,\mathrm{d}t = \frac{1}{\eta}\left(\int_0^\infty I(x)\,\mathrm{d}x\right)\,\mathrm{d}S\,\mathrm{d}t \tag{2}$$

where J is the flux density, η is the efficiency of the injection process and $I(x)$ describes the depth distribution of the injected particles. The trapping probability in the thin layer $\mathrm{d}x$ is equal to the ratio of the expressions (1) and (2):

$$\frac{z\nu c(x)}{N_0 J} n(x)\,\mathrm{d}x \equiv \mu(x) n(x)\,\mathrm{d}x. \tag{3}$$

The steady-state concentration of mobile particles, $c(x)$, follows from the balance between diffusion, production and trapping:

$$D\frac{\partial^2 c}{\partial x^2} + I(x) - \mu(x) n(x) J = 0. \tag{4}$$

If we can neglect the effect of trapping, the solution is given by

$$Dc(x) = \int_0^x \xi I(\xi)\,\mathrm{d}\xi + x\int_x^\infty I(\xi)\,\mathrm{d}\xi. \tag{5}$$

The second term in equation (5) disappears at large depths, provided that $I(\xi) \simeq \xi^{-k}$ with $k > 2$. For x beyond the average deposition depth $\langle x\rangle$ we have, therefore,

$$Dc(x) \simeq \langle x\rangle \int_0^\infty I(\xi)\,\mathrm{d}\xi = \eta\langle x\rangle J \tag{6}$$

$$\mu(x) \simeq \frac{z\eta\langle x\rangle}{\Gamma\lambda^2 N_0}. \tag{7}$$

We used the relation $D = \Gamma\lambda^2\nu$, where Γ is a geometrical factor and λ is the length of an elementary jump. Under these restrictions, the factor $\mu(x)$ is constant and may be considered to be the cross section for trapping at a depth x.

Equation (7) is only valid if the trapping term in the balance equation (4) may be neglected. However, our samples were prepared by room-temperature implantation of ^{111}In into tungsten to a dose of 1×10^{12} cm^{-2}, at an implantation energy of 50 keV. For this case we calculate about 2×10^{14} cm^{-2} vacancies from the modified Kinchin–Pease formula, assuming that 20% of the created vacancies survive recovery stage III. The trapping cross section is estimated to be 2×10^{-13} cm^2 using the parameter values $z = 1$, $\eta = 0.57$, $\langle x\rangle = 15a$ (from a TRIM simulation), $\Gamma = 1/6$, $\lambda^2 = a^2/8$, $N_0 = 2/a^3$ and $a = 3.16$ Å. Hence, the ratio of trapping and production is $2\times10^{14}\times2\times10^{-13} = 40$, and the trapping term may not be neglected.

To illustrate this, we solved equation (4), assuming the boundary conditions $c(0) = 0$ and $c'(\infty) = 0$. The hydrogen implantation profile shall be a Gaussian with an average depth of $x_H = 15a$ and a straggling of $\sigma_H = 8a$. The traps, introduced by a 50 keV ^{111}In implantation, shall be distributed according to a Gaussian profile with an average depth $x_n = 60a$ and a straggling of $\sigma_n = 20a$. The integration is started at large depth, and a properly normalized solution of the homogeneous equation is added to the result in order to satisfy the boundary condition at the surface. The hydrogen concentration and, hence, the trapping cross section turn out to be strongly suppressed in the region of the damage cascade if the total number of vacancies exceeds 10^{12} cm^{-2}. One may define an effective trapping cross section as

$$\mu_{\text{eff}} = \int \mu(x)n(x)\,\mathrm{d}x \Big/ \int n(x)\,\mathrm{d}x. \tag{8}$$

The reduction factor μ_{eff}/μ is roughly inversely proportional to the total number of traps if $n \gg 10^{12}$ cm^{-2}, as shown in figure 1.

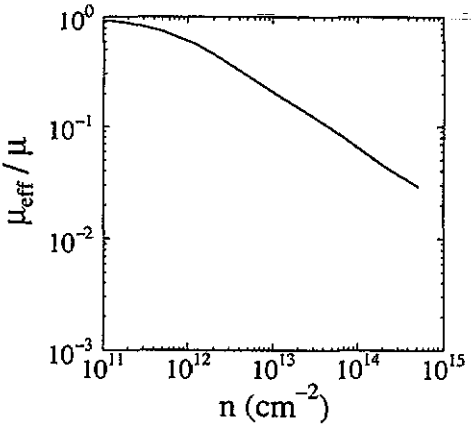

Figure 1. The reduction factor μ_{eff}/μ as a function of the integrated trap density n.

3. Perturbed angular correlation of γ-rays

Before considering the experimental results, we describe in heuristic terms the essential features of the perturbed angular correlation technique. For a more complete treatment of nuclear radiations, their correlations, and extra-nuclear perturbations, we refer the reader to the existing literature (Steffen and Alder 1975, Wichert and Recknagel 1986).

Basic to the method is the selection of an ensemble of excited nuclei with unequal populations of magnetic substates. As such states decay, the probability for γ-ray emission will have an anisotropic distribution with respect to the axis of quantization. In the absence of hyperfine interations, the directional distribution of the γ-rays will be given by

$$W(\theta) = 1 + A_2 P_2(\cos\theta) + \cdots \tag{9}$$

where the ellipsis indicates higher-order terms and θ is the angle between the axis of quantization and the direction of the emitted γ quantum. The anisotropy coefficient A_2 depends on the population imbalance among the magnetic substates and the multipolarity of the emitted γ-ray. Neglect of higher-order terms is justified in the case of the nuclear probe ^{111}In.

In the presence of hyperfine interactions, the directional distribution becomes time-dependent with the form

$$W(\theta, t) = 1 + A_2 \hat{G}_2(\theta, t) + \cdots. \tag{10}$$

The so-called perturbation function $\hat{G}_2(\theta, t)$ contains all relevant information about the interaction of nuclear moments with extra-nuclear fields. If the perturbation is due to an electric quadrupole interaction with axial symmetry and random orientation, and the nuclear spin is $I = 5/2$, we have

$$\begin{aligned} \hat{G}_2(\theta, t) &= G_2(t) P_2(\cos\theta) \\ G_2(t) &= \tfrac{1}{5}(1 + \tfrac{13}{7}\cos\omega_0 t + \tfrac{10}{7}\cos 2\omega_0 t + \tfrac{5}{7}\cos 3\omega_0 t) \end{aligned} \tag{11}$$

where $\omega_0 = (3\pi/10)eQV_{zz}/h$. Here, Q is the nuclear electric quadrupole moment, and V_{zz} is the z-component of the diagonalized electric field gradient tensor. In defect studies, the discrete quadrupole frequency ω_0 is used to 'flag' a particular defect state for identification in subsequent observations.

To select the unequal populations of m states required for these effects, a coincidence measurement is made on a $\gamma\gamma$ cascade. Detecting the first γ-ray in a given direction selects a preferred nuclear spin direction, and ensures that the second γ-ray has an anisotropic distribution. The coincident count rate as a function of the time lag t between the detection of the first and the second γ-ray can be written as

$$C_{ij}(\theta, t) = C_{ij} e^{-t/\tau_N} W(\theta, t) + B_{ij} \tag{12}$$

where C_{ij} and B_{ij} are the true and accidental coincidence count rates, τ_N is the lifetime of the intermediate nuclear level. The angle θ between the detectors i and j in our experiments was either 90° or 180°. To eliminate the exponential decay factor

as well as the effects of detector efficiencies and finite solid angles subtended by the γ-ray detectors, we formed the following ratio (Arends *et al* 1980).

$$R(t)_{\text{exp}} = \frac{C_{180} - C_{90}}{\frac{1}{2}C_{180} + C_{90}} \tag{13}$$

where C_{90} and C_{180} are the averaged and background-corrected count rates for the 90° and 180° detector combinations

$$\begin{aligned} C_{90} &= \sqrt{\{C_{14}(90°,t) - B_{14}\}\{C_{23}(90°,t) - B_{23}\}} \\ C_{180} &= \sqrt{\{C_{13}(180°,t) - B_{13}\}\{C_{24}(180°,t) - B_{24}\}}. \end{aligned} \tag{14}$$

Provided the effective anisotropy is the same for all detector pairs, the theoretically expected value of the right-hand side of equation (13) is

$$R(t)_{\text{theo}} = A_{\text{eff}}G(t). \tag{15}$$

To determine the frequencies and the relative numbers of distinct defects, the experimental ratio $R(t)_{\text{exp}}$ was least-squares fitted with the expression:

$$F(t) = f_0 + \Sigma_m f_m G(\omega_{0m}, \delta_m, \eta_m, t). \tag{16}$$

The sum over m accounts for the contribution of different defect sites to $R(t)$ and

$$G(\omega_0, \delta, \eta, t) = \Sigma_n s_n(\eta) h\{g_n(\eta)\delta t\} \cos\{g_n(\eta)\omega_0 t\}. \tag{17}$$

The function $h(z)$, which is taken to be either a Gaussian or an exponential function, describes a possible distribution of quadrupole frequencies. The deviation of the electric field gradient tensor from axial symmetry is given by the asymmetry parameter $\eta = (V_{xx} - V_{yy})/V_{zz}$ with $|V_{xx}| \leqslant |V_{yy}| \leqslant |V_{zz}|$. The relative amplitudes, $s_n(\eta)$, and the relative frequencies, $g_n(\eta)$, in equation (17) depend in a known way on η. It is generally believed that the symmetry of the electric field gradient tensor reflects the symmetry of the defect structure.

4. Experimental details

For all our measurements we used polycrystalline tungsten foils with a purity of 99.95%. After having been annealed in vacuum ($p \approx 1 \times 10^{-6}$ mbar) at 1273 K for 30 min to remove the tungsten oxide layer, they were implanted with 50 keV ^{111}In ions to a dose of $\leqslant 1 \times 10^{12}$ cm^{-2}. The effect of subsequent annealing is demonstrated in figure 2, where the Fourier transform of the perturbation function is shown as measured after annealing for 15 min at different temperatures. The quadrupole frequencies 133 Mrad s^{-1}, 301 Mrad s^{-1} and 249 Mrad s^{-1} have been assigned to InV_2, InV_3 and microvoids, respectively (Post *et al* 1983, Van der Kolk *et al* 1985, Pütz *et al* 1986). From this figure it is clear that after annealing at 750 K only one distinct defect is visible. This standard treatment creates a well defined situation with about 20% of the ^{111}In ions located in InV_2 complexes. Of the remaining In atoms, about

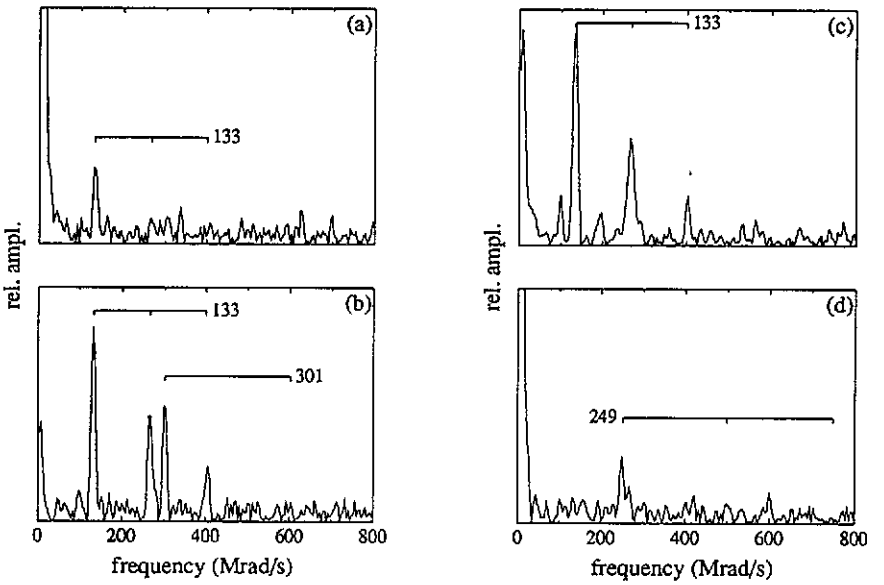

Figure 2. Fourier transform of the perturbation function measured (*a*) after 50 keV ^{111}In implantation at RT, and after subsequent annealing at (*b*) 620, (*c*) 750 and (*d*) 820 K. The quadrupole frequencies 133 Mrad s^{-1}, 301 Mrad s^{-1} and 249 Mrad s^{-1} correspond to InV_2, InV_3 and microvoids, respectively (Post *et al* 1983, Van der Kolk *et al* 1985, Pütz *et al* 1986).

20% are at substitutional lattice sites in an unperturbed environment, while the others are probably located in small vacancy clusters containing four or more vacancies. Next, the samples were implanted with 1 keV hydrogen molecules corresponding to 500 eV H^+ ions, using a low-energy ion gun. The maximum energy transferred in this case to the lattice amounts to 11 eV, which is well below the minimum displacement energy. Therefore, no further damage is introduced into the samples by the hydrogen implantations.

In our experiments we varied the hydrogen dose from 1×10^{13} up to 1×10^{17} cm^{-2}. To study the stability of the hydrogen decorated defects, we performed an annealing sequence on samples that had been implanted with 5×10^{15} H cm^{-2}. For temperatures up to 398 K the samples were annealed 'au bain-marie', and at higher temperatures they were annealed in vacuum ($p \approx 1 \times 10^{-6}$ mbar). The annealing time was 15 min in all cases. Other samples implanted with a hydrogen dose of 5×10^{15} cm^{-2} were mounted on the tip of a helium flow-cryostat in order to study the temperature dependence of the electric field gradients. The temperature of the samples was varied from 25 K to room temperature (RT).

The PAC spectra were measured using four γ-ray detectors positioned at relative angles of 90° and 180°. Each detector consisted of a 51 mm x 45 mm diameter NaI(Tl) scintillator mounted onto an RCA 8575 photomultiplier. The time resolution of the system was about 3 ns FWHM resulting in an accessible frequency domain of about 1 Grad s^{-1}.

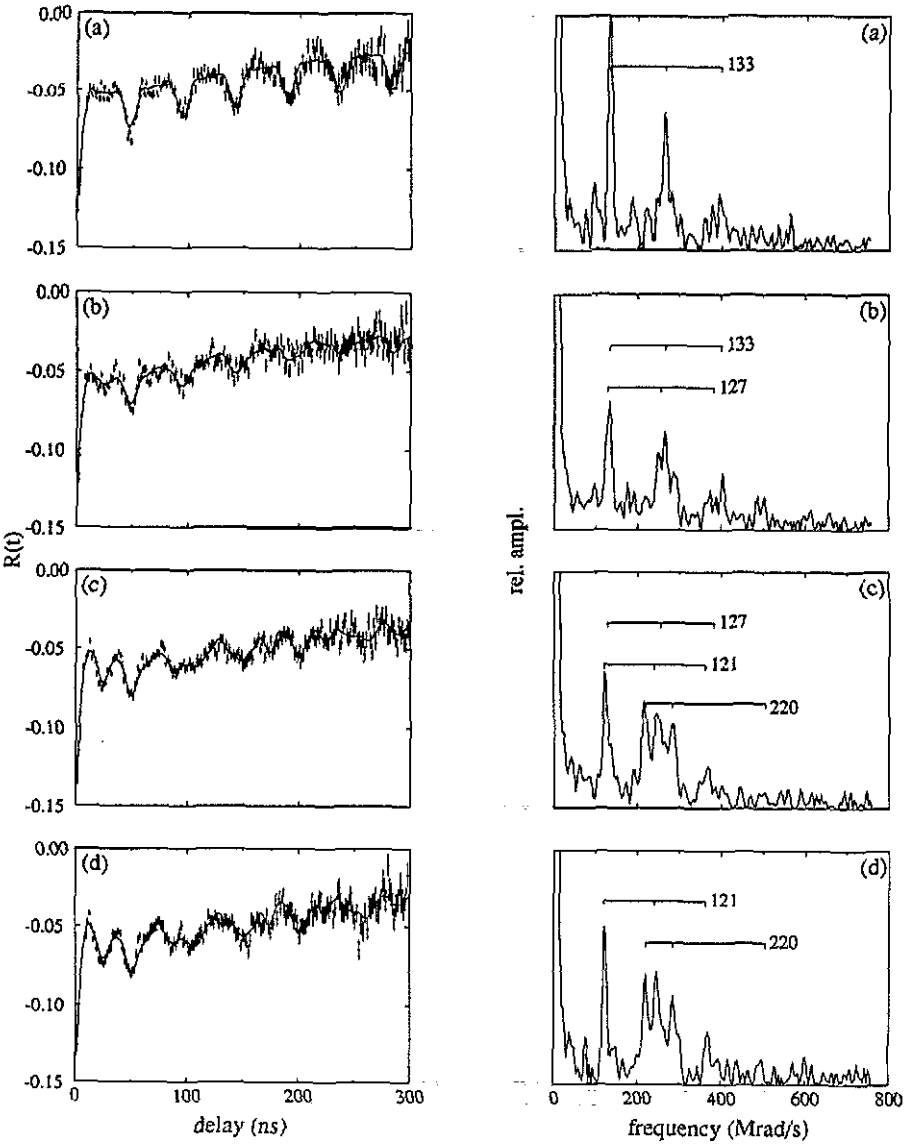

Figure 3. PAC *spectra (left) and their Fourier transforms (right) measured (a) before hydrogen implantation, and after hydrogen implantation to a dose of (b)* 1×10^{14}, *(c)* 3×10^{15} *and (d)* 9×10^{16} cm^{-2}.

5. Experimental results

After the standard treatment described previously, only one single component is visible in the Fourier transform of the PAC spectrum. Frequency and asymmetry parameter, $\omega_0 = 133$ *Mrad* s^{-1} *with* $\eta = 0$, of this component correspond to the InV_2 defect, the fraction being approximately 20%.

After hydrogen implantation the Fourier spectra become much more complicated. The number of undecorated vacancies decreases and new defects appear. In figure 3 we

show some typical PAC spectra and their Fourier transforms that were obtained after implantation of hydrogen to the specified doses. The frequency of the InV_2 defect changes to a smaller value and extra peaks appear in the Fourier spectra around approximately 220 Mrad s^{-1}. After a careful analysis of a series of measurements it became clear that the frequency of the InV_2 defect shifts from 133 via 127 to 121 Mrad s^{-1}, with increasing hydrogen dose, indicating the formation of at least two different defect structures. The asymmetry parameter, however, remains zero. The peaks in the Fourier transform at 220 Mrad s^{-1} could be fitted reasonably well assuming one component with a frequency of about 220 Mrad s^{-1} and an asymmetry parameter $\eta \simeq 0.7$.

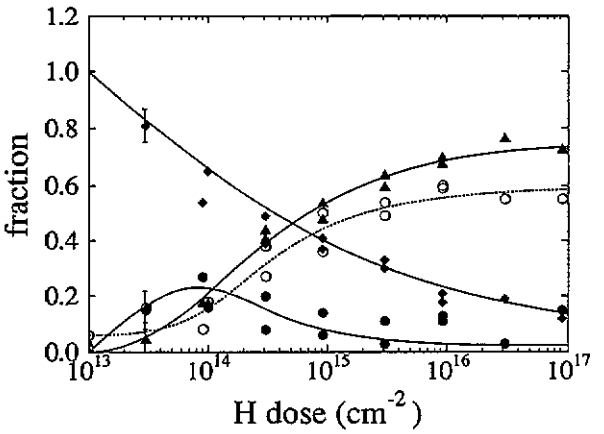

Figure 4. Normalized fractions of the different defects as a function of the hydrogen dose: ♦, 133; ●, 127; ▲, 121; and ○, 220 Mrad s^{-1}. The bars in the data points for a hydrogen dose of 3×10^{13} cm^{-2} give an indication of the accuracy of the results. The curves are a guide to the eye.

The fitting procedure was as follows. The frequency corresponding with the bare vacancy, 133 Mrad s^{-1}, was kept fixed at the value measured on the undoped samples. The frequency of 121 Mrad s^{-1} was obtained from summed spectra taken in the region of large hydrogen doses. These frequencies being known, we obtained the intermediate frequency, 127 Mrad s^{-1}, by summing the spectra taken at a hydrogen dose of about 10^{14} cm^{-2}. Finally, the fractions of the different defects were determined by fitting each individual spectrum with four components, the triplet of 133, 127 and 121 Mrad s^{-1} and the 220 Mrad s^{-1} defect, while keeping the frequencies of the triplet fixed at the previously obtained values. The results were normalized to the sum of the fractions of the 133, 127 and 121 Mrad s^{-1} defects, which amounted to 16% and 13% for the two different samples used in the experiment, and stayed approximately constant as a function of hydrogen dose. The final result is shown in figure 4.

The thermal stability of the hydrogen decorated defects was investigated by performing a thermal annealing sequence. The PAC spectra and their Fourier transforms obtained after annealing at 348, 398 and 623 K are shown in figure 5. It follows that the defect that gives rise to frequencies around 220 Mrad s^{-1} is the least stable of all. At the end of the annealing sequence the original InV_2 defect reappeared. The different defect fractions were calculated in the same way as in the case of the dose experiments, yielding the results shown in figure 6.

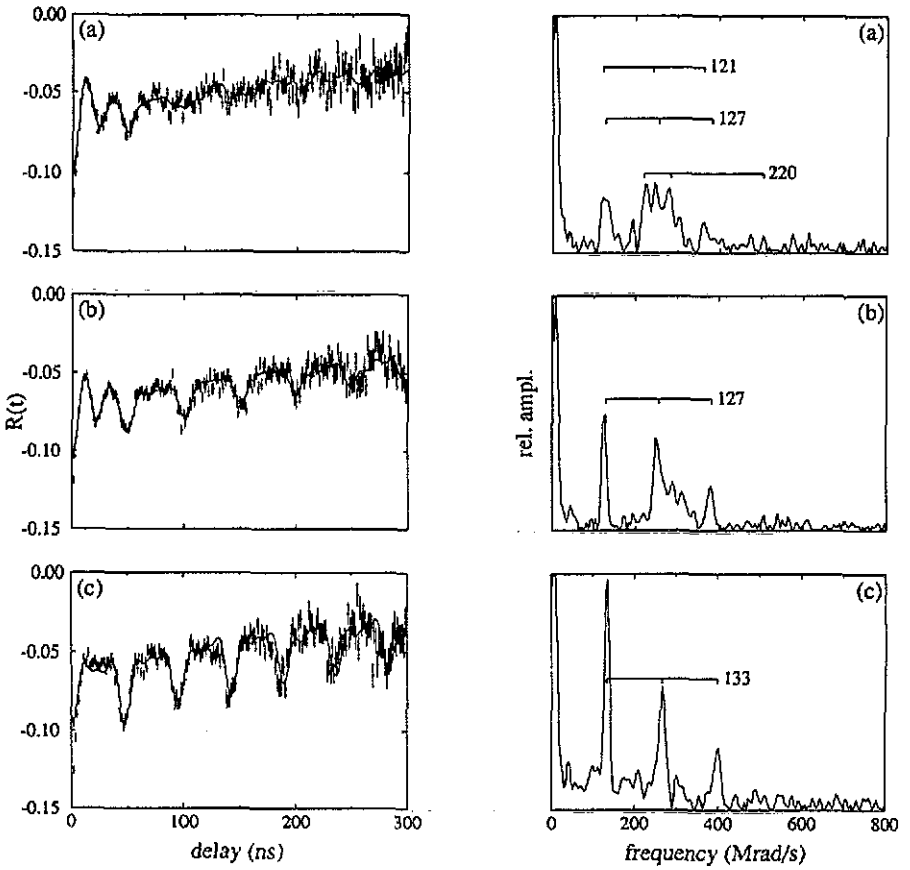

Figure 5. PAC spectra (left) and their Fourier transforms (right) measured after hydrogen implantation to a dose of 5×10^{15} cm^{-2} and subsequent annealing at (*a*) 348, (*b*) 398 and (*c*) 623 K.

We finally measured the temperature dependence of the different hyperfine interactions for temperatures between 25 K and RT, using a sample that had been prepared according to the standard procedure and was implanted with hydrogen to a dose of 5×10^{15} cm^{-2}. From these measurements it became clear that the Fourier peaks at 220 Mrad s^{-1} had to be fitted with two sets of frequencies. We further included the '133–127–121 Mrad s^{-1} triplet' in the fit. In this case, the amplitudes were fixed at the average value, while the frequencies were varied. The results shown in figure 7 demonstrate that the three lower frequencies are almost constant as a function of temperature, whereas the two higher frequencies are not. From the analysis we derived the following values for the doublet around 220 Mrad s^{-1}: (i) 216 Mrad s^{-1} and $\eta = 0.65$ at $T_m = 25$ K changing to 221 Mrad s^{-1} and $\eta = 0.72$ at $T_m = 300$ K, and (ii) 238 Mrad s^{-1} at $T_m = 25$ K changing to 228 Mrad s^{-1} at $T_m = 300$ K with an approximately constant $\eta = 0.72$.

To prove that the members of the '133–127–121 Mrad s^{-1} triplet' are generically related, we implanted a hydrogen dose of 1×10^{16} cm^{-2} into tungsten foils which had been annealed at RT or at 820 K (see figure 2). After annealing at these temperatures,

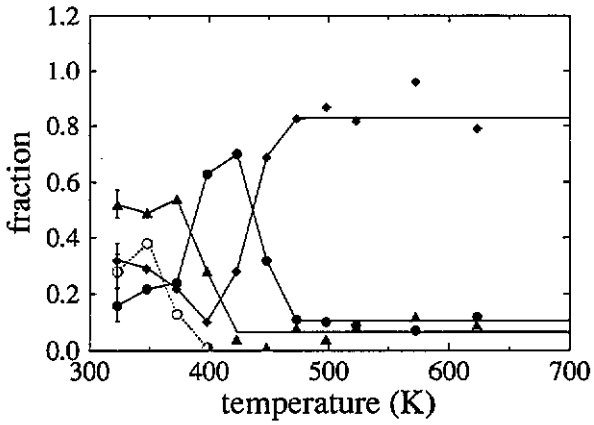

Figure 6. Calculated fractions of the different defects as a function of the annealing temperature: ♦, 133; ●, 127; ▲, 121; and ○, 220 Mrad s^{-1}. The fractions are normalized to the sum of the first three fractions.

the InV_3 fraction was less than 1%; InV_2 was only observed in the as-implanted sample, with a fraction of about 5%. Implantation of hydrogen did not have any measurable effect. Therefore, no ^{111}In containing hydrogen traps were available in these samples. This observation indicates in particular that substitutional ^{111}In in tungsten does not trap hydrogen at room temperature.

6. Discussion

From the measurements described previously we have derived a triplet of quadrupole interactions. The frequency changed from the original value of 133 Mrad s^{-1} via 127 to 121 Mrad s^{-1} with increasing hydrogen dose, while the asymmetry parameter is zero in all three cases. On further implantation of hydrogen the frequency did not change by more than 0.5 Mrad s^{-1}. We also observed a frequency distribution around 220 Mrad s^{-1}, which could be attributed to at least two distinct defects, both giving rise to an electric field gradient with an asymmetry parameter of approximately 0.7. This suggests that after hydrogen decoration at least four new defect structures are formed. In the following discussion we will first address the nature of the defects giving rise to the triplet of frequencies and then deal with the defects causing the frequency doublet.

6.1. Structure of the hydrogen decorated vacancy

A straightforward explanation of the triplet would be the decoration of InV_2 with one and two hydrogen atoms, respectively, according to the following reaction

$$InV_2 + 2H \rightarrow InV_2H + H \rightarrow InV_2H_2. \tag{18}$$

The fact that in preliminary work (Post and Pleiter 1987, Fransens *et al* 1988) the 121 and 127 Mrad s^{-1} components were not resolved is probably due to the circumstance that at that time it was not possible to vary the hydrogen dose in a controlled way.

In order to see whether the deduced change of the quadrupole frequency by $\Delta\omega_0 = -6$ Mrad s^{-1} per hydrogen atom is a realistic value, we estimated this change using

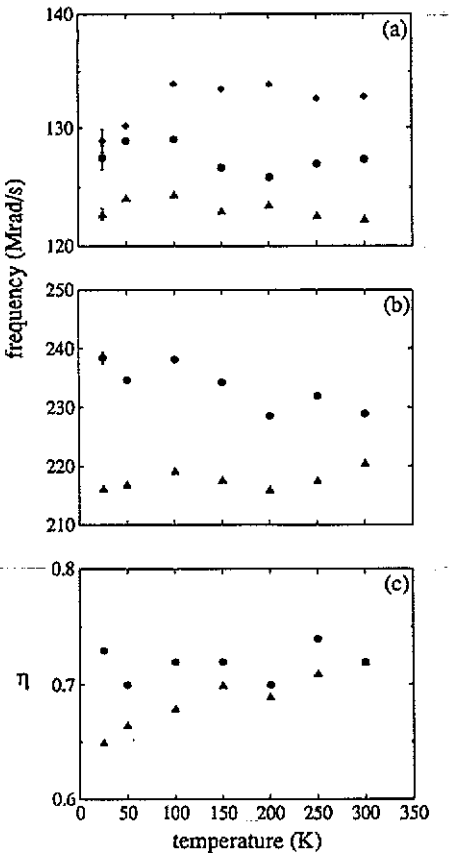

Figure 7. Temperature dependence of (*a*) the 133, 127 and 121 Mrad s^{-1} frequencies, and of (*b*) the two frequencies at about 220 Mrad s^{-1} and (*c*) the values of the corresponding asymmetry parameters.

the point charge model. For the effective charge of the hydrogen atoms we took a value of $+0.33e$, obtained from the measured electric field gradients in a number of metal hydrides (Weidinger 1984). From the observed quadrupole frequency of the InV_2 defect we derived a value of $-1.8e$ for the effective charge of the vacancy in tungsten. The calculated values of ω_0 and η for the case of a single hydrogen atom at the different tetrahedral and octahedral positions around the InV_2 complex are shown in figure 8. Evidently, the hydrogen atom cannot be positioned too close to the ^{111}In atom, even not if we accept a deviation of 3 Mrad s^{-1} from the measured value of 127 Mrad s^{-1} and values for the asymmetry parameter up to 0.1. It is also clear that we cannot discriminate between the different hydrogen trap locations on the basis of the hyperfine interactions. To calculate the effect of multiple hydrogen decoration, a second hydrogen atom was added to the other side of the vacancy compared with the first hydrogen atom, which is energetically the most favourable position. The calculated effect of additional hydrogen atoms positioned on either tetrahedral or octahedral positions is an approximately linear decrease of the quadrupole frequency as long as the hydrogen atoms are not located too close to the ^{111}In atom. It is

reasonable, therefore, to conclude that InV_2 traps only one or two hydrogen atoms at RT.

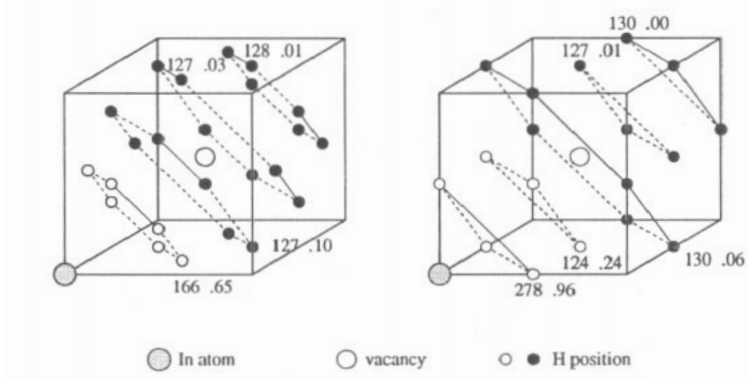

Figure 8. Calculated values of the quadrupole frequency and asymmetry parameter for the InV_2 defect decorated with one hydrogen atom on a tetrahedral position (left) or an octahedral position (right). Only one out of a number of equivalent sites in the same (111) plane is labelled. The open circles indicate positions that do not fulfil the acceptance criteria (see text).

Additional support for this interpretation is obtained from the change of the 127 Mrad s^{-1} fraction as a function of hydrogen dose and annealing temperature. Figure 4 shows that for low hydrogen doses this defect fraction increases, whereas it decreases at higher hydrogen doses in favour of the 121 Mrad s^{-1} defect. In a model in which the trapping probability does not depend on the number of hydrogen atoms already trapped, the number of defects with n trapped hydrogen atoms is always smaller than the number of defects which have trapped $n-1$ hydrogen atoms. Such a model can reproduce the large fraction of the 121 Mrad s^{-1} defect only if the frequency is assumed not to decrease further when more than two hydrogen atoms are trapped. This, however, disagrees with the results of the point charge calculations described before.

Figure 6 shows that during annealing at about 400 K the 121 and the 133 Mrad s^{-1} fractions decrease, while the 127 Mrad s^{-1} fraction increases. The explanation of this behaviour in terms of single and double hydrogen decoration of the InV_2 defect is straightforward: one of the two hydrogen atoms is released from the complex and is either trapped at InV_2 or at one of the larger vacancy clusters, or it escapes to the surface. Therefore, the 127 Mrad s^{-1} fraction should increase and the 133 Mrad s^{-1} fraction should decrease, as is indeed observed. During annealing of the sample at about 450 K also the last hydrogen atom is released, resulting in a further increase of the InV_2 fraction and the disappearance of the 127 Mrad s^{-1} fraction. The fact that even at the highest annealing temperatures a small fraction of decorated defects is found is an artefact of the fitting procedure.

The measurements at different sample temperatures showed that the Fourier peaks at 220 Mrad s^{-1} are due to at least two different defects. There are some indications that these defects contain large amounts of hydrogen. The first indications come from the observed additional hydrogen trapping when the '220 Mrad s^{-1}' defect dissociates at about 370 K, leading to a further reduction of the number of undecorated InV_2 clusters. A further clue is obtained from the decrease of the cross section (see figure 9).

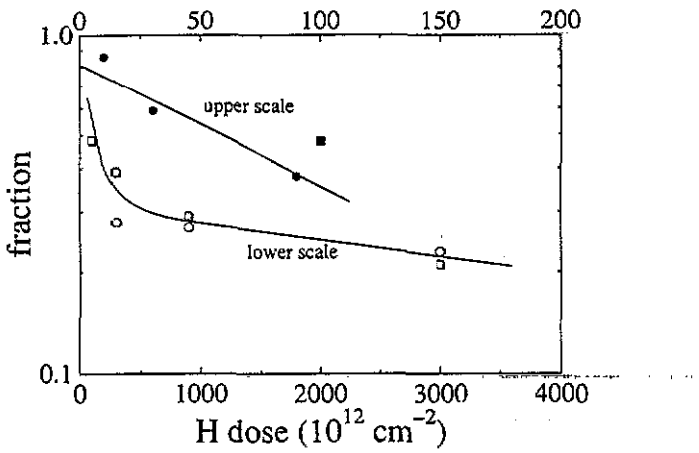

Figure 9. Normalized InV_2 fraction as a function of the hydrogen dose.

The initial value of $\mu = 4 \times 10^{-15}$ cm^2 decreases to $\mu = 3 \times 10^{-17}$ cm^2 at higher hydrogen doses, indicating the formation of strong competitive hydrogen traps. In section 2 we estimated a value $\mu = 2 \times 10^{-13}$ cm^2. Taking into account the fact that the number of traps is roughly 2×10^{14} cm^{-2}, we obtain from figure 1 an effective trapping cross section $\mu_{\text{eff}} = 4 \times 10^{-2}\mu = 8.0 \times 10^{-15}$ cm^2, which is in good agreement with the value of μ measured for small hydrogen doses.

The origin of the '220 Mrad s^{-1}' defects has still to be clarified. After ^{111}In implantation and subsequent annealing at 750 K we only observe the InV_2 defect. Since the sum of the InV_2 fraction and the fractions of decorated InV_2 clusters is nearly constant, it is not possible that the '220 Mrad s^{-1}' defect is generically related to InV_2. The decoration measurements on samples annealed at either room temperature or at 820 K clearly showed that substitutional ^{111}In does not trap hydrogen at room temperature. Substitutional ^{111}In and InV_2 defects being ruled out, the only possible seeds for the '220 Mrad s^{-1}' defects are larger In–vacancy clusters. These clusters give rise to a distribution of quadrupole frequencies and are, therefore, hardly visible in the Fourier transform of the perturbation factor.

6.2. Hydrogen–vacancy binding energy

Assuming a single-step detrapping process, we may calculate the desorption energy for the first and second hydrogen atom from the expression

$$E_d = k_B T_d \ln(\nu_0 t / \ln 2) \tag{19}$$

where $t = 900$ s is the annealing time and ν_0 the attempt frequency. From the experimental value of the hydrogen diffusion coefficient, $D_0 = 4.1 \times 10^{-13}$ cm^2 s^{-1} (Frauenfelder 1969), the relation $D_0 = \Gamma\lambda^2\nu_0, \Gamma = 1/6, \lambda^2 = a^2/8$ and $a = 3.16$ Å, we find $\nu_0 = 2.0 \times 10^{14}$ s^{-1}. Taking a value for T_d for which the fraction is reduced by 50%, we get $E_d = 1.38(2)$ eV and $E_d = 1.55(2)$ eV for the detrapping energy of the second and the first hydrogen atom from InV_2H_2. The error accounts merely for the uncertainty in the value of the detrapping temperature, T_d. Using a value of 0.39 eV for the hydrogen migration energy in tungsten (Frauenfelder 1969), we obtain the binding energies $E_b = 0.99(2)$ eV and $E_b = 1.16(2)$ eV, respectively,

which are in good agreement with the values quoted in table 1. Trapping of a third hydrogen atom was not observed. If such an atom had trapped, it must therefore have detrapped within a time which is short compared with the typical time required for taking a PAC spectrum. From this we estimate that the dissociation energy for the third hydrogen atom is less than 1.1 eV. Finally, the dissociation energy of the bubble-like '220 Mrad s^{-1}' defect is 1.30(2) eV.

Table 1. Calculated binding energy, E_b^i, for the ith hydrogen or deuterium atom at a vacancy in several BCC metals. All values in eV.

Metal	Hydrogen[a]	Deuterium[b]					
	E_b^1	E_b^1	E_b^2	E_b^3	E_b^4	E_b^5	E_b^6
Fe	0.86	0.83	0.79	0.54	0.51	0.41	0.42
Nb	0.51	0.59	0.56	0.61	0.53	0.52	0.55
Mo	0.92	0.96	0.95	0.80	0.73	0.71	0.70
W	1.15	—	—	—	—	—	—

[a] Nordlander *et al* 1986.
[b] Nordlander *et al* 1989.

The difference of 0.17 eV between the binding energies of the first and second hydrogen atom disagrees with the predictions of the effective-medium theory (see table 1), but nicely agrees with the energy difference of 0.23 eV obtained from the analysis of deuterium depth profiles in molybdenum (Myers and Besenbacher 1986). On the basis of the theoretical predictions one might argue that the detrapping stages at 400 and 450 K (see figure 6) each correspond to the release of two hydrogen atoms. This would not be in contradiction with the point-charge model, which merely states that equal changes of the electric field gradient must be related to trapping or detrapping of equal numbers of hydrogen atoms. However, it necessarily implies that the fifth hydrogen atom binds much weaker to the vacancy than the preceding one, which would lead to another conflict with the effective-medium theory.

Detrapped hydrogen can be retrapped at deeper traps in the neighbourhood, making it impossible for the hydrogen to escape from the damage region. Retrapping plays, therefore, an important role in the interpretation of measured depth profiles (Myers and Besenbacher 1986). However, in our experiments retrapping cannot hamper the analysis. If hydrogen detraps from InV_2 and retraps at a deeper trap, it remains unobserved because it is no longer attached to the probe atom ^{111}In. The sharp increase and decrease of the defect fractions as a function of the annealing temperature provide further evidence that the InV_2 clusters do not retrap the hydrogen atoms once they have been released.

7. Conclusions

Our perturbed angular correlation measurements show that a vacancy in tungsten can trap one or two hydrogen atoms at room temperature. The detrapping energies of the first and second hydrogen atom are 1.55(2) and 1.38(2) eV, respectively, while the detrapping energy of the next hydrogen atom is less than 1.1 eV. Substitutional ^{111}In atoms do not trap hydrogen at room temperature. At least two more hydrogen decorated defects were observed. Although their structures are not quite clear,

they probably form from larger vacancy clusters and may contain a large amount of hydrogen. The dissociation energy of these bubble-like defects is 1.30(2) eV.

Acknowledgments

This work was performed as a part of the research programme of the Stichting voor Fundamenteel Onderzoek der Materie (FOM), with financial support from the Nederlandse Organisatie voor Wetenschappelijk Onderzoek (NWO). One of us (M S Abd El Keriem) gratefully acknowledges the scholarship granted by the Egyptian Minister of Higher Education.

References

Arends A R, Hohenemser C, Pleiter F, De Waard H, Chow L and Suter R M 1980 *Hyperfine Interact.* **8** 191

Besenbacher F, Myers S M and Nørskov J K 1985 *Nucl. Instrum. Methods* B **7/8** 55

Fransens J R, Pleiter F and Schlatmann B 1988 *Condensed Matter Studied by Nuclear Methods* vol 2, ed K Królas and K Tomala (Kraków: Institut of Nuclear Physics) pp 315

Frauenfelder R 1969 *J. Vac. Sci. Technol.* **6** 388

Hansen H E, Talja R, Rajainmäki H, Nielsen H K, Nielsen B and Nieminen R M 1985 *Appl. Phys.* A **36** 81

Ligeon E, Danielon R, Fontenille J and Eymery R 1986 *J. Appl. Phys.* **59** 108

Linderoth S, Rajainmäki H, Nielsen B, Hansen H E, Nieminen R M and Petersen K 1987 *Proc. Int. Conf. on Vacancies and Interstitials in Metals and Alloys (Materials Science Forum 15–18)* ed C Abromeit and H Wollenberger (Aedermannsdorf: Trans. Tech.) p 751

Myers S M and Besenbacher F 1986 *J. Appl. Phys.* **60** 3499

Nordlander P, Nørskov J K and Besenbacher F 1986 *J. Phys. F: Met. Phys.* **16** 1161

Nordlander P, Nørskov J K, Besenbacher F and Myers S M 1989 *Phys. Rev.* B **40** 1990

Picraux S T 1976 *Ion Beam Surface Analysis* vol 2, ed O Meyer, G Linker and F Käppler (New York: Plenum) p 527

Picraux S T and Vook F L 1974 *Phys. Rev. Lett.* **33** 1216

Post K and Pleiter F 1987 *Hyperfine Interact.* **35** 615

Post K, Pleiter F, Van der Kolk G J, Van Veen A, Caspers L M and De Hosson J Th M 1983 *Hyperfine Interact.* **15/16** 421

Puska M J and Nieminen R M 1984 *Phys. Rev.* B **29** 5382

Pütz U, Hoffmann A, Rudolph H J and Vianden R 1986 *Z. Phys.* B **46** 107

Steffen R M and Alder K 1975 *The Electromagnetic Interaction in Nuclear Spectroscopy* ed W D Hamilton (Amsterdam: North-Holland) ch 12–13

Van der Kolk G J, Post K, Van Veen A, Pleiter F and De Hosson J Th M 1985 *Radiat. Eff.* **84** 131

Van Gorkum A A and Kornelsen E V 1979 *Radiat. Eff.* **42** 93

Van Veen A and Caspers L M 1980 *Harwell Symposium on Inert Gases in Metals and Ionic Solids* ed S F Pugh *AERE Report* 9733, p 517

Weidinger A 1984 *J. Less-Common Met.* **103** 285

Wichert Th and Recknagel E 1986 *Microscopic Methods in Metals (Topics in Current Physics 40)* ed U Gonser (Berlin: Springer) p 317